ENVIRONMENTAL RESEARCH
LETTERS

PURPOSE-LED PUBLISHING™

LETTER • OPEN ACCESS

Mixing and dilution controls on marine CO_2 removal using alkalinity enhancement

To cite this article: Tarang Khangaonkar *et al* 2024 *Environ. Res. Lett.* **19** 104039

ENVIRONMENTAL RESEARCH
LETTERS

LETTER

Mixing and dilution controls on marine CO_2 removal using alkalinity enhancement

Tarang Khangaonkar[1,2,*], **Brendan R Carter**[2,3], **Lakshitha Premathilake**[1,2], **Su Kyong Yun**[1], **Wenfei Ni**[1], **Mary Margaret Stoll**[2], **Nicholas D Ward**[4], **Lenaïg G Hemery**[4], **Carolina Torres Sanchez**[4], **Chinmayee V Subban**[1], **Mallory C Ringham**[7], **Matthew D Eisaman**[5,6], **Todd Pelman**[7], **Krti Tallam**[7] and **Richard A Feely**[3]

[1] Energy and Environment Directorate, Pacific Northwest National Laboratory, Seattle, WA 98109, United States of America
[2] University of Washington, Seattle, WA, United States of America
[3] Pacific Marine Environmental Laboratory, NOAA, Seattle, WA, United States of America
[4] Marine and Coastal Research Laboratory, PNNL, Sequim, WA, United States of America
[5] Department of Earth & Planetary Sciences, Yale University, New Haven, CT, United States of America
[6] Yale Center for Natural Carbon Capture, Yale University, New Haven, CT, United States of America
[7] Ebb Carbon, Inc., San Carlos, CA, United States of America
[*] Author to whom any correspondence should be addressed.

E-mail: Tarang.Khangaonkar@pnnl.gov

OPEN ACCESS

RECEIVED
6 June 2024

REVISED
26 August 2024

ACCEPTED FOR PUBLICATION
29 August 2024

PUBLISHED
6 September 2024

Keywords: ocean alkalinity enhancement, modeling, marine carbon dioxide removal, zone of influence, mixing, dilution, carbon dioxide outgassing reduction

Supplementary material for this article is available online

Abstract

Marine CO_2 removal (CDR) using enhanced-alkalinity seawater discharge was simulated in the estuarine waters of the Salish Sea, Washington, US. The high-alkalinity seawater would be generated using bipolar membrane electrodialysis technology to remove acid and the alkaline stream returned to the sea. Response of the receiving waters was evaluated using a shoreline resolving hydrodynamic model with biogeochemistry, and carbonate chemistry. Two sites, and two deployment scales, each with enhanced TA of 2997 mmol m^{-3} and a pH of 9 were simulated. The effects on air-sea CO_2 flux and pH in the near-field as well as over the larger estuary wide domain were assessed. The large-scale deployment (addition of 164 Mmoles TA yr^{-1}) in a small embayment (Sequim Bay, 12.5 km^2) resulted in removal of 2066 T of CO_2 (45% of total simulated) at rate of 3756 mmol m^{-2} yr^{-1}, higher than the 63 mmol m^{-2} yr^{-1} required globally to remove 1.0 GT CO_2 yr^{-1}. It also reduced acidity in the bay, $\Delta pH \approx +0.1$ pH units, an amount comparable to the historic impacts of anthropogenic acidification in the Salish Sea. The mixing and dilution of added TA with distance from the source results in reduced CDR rates such that comparable amount 2176 T CO_2 yr^{-1} was removed over >1000 fold larger area of the rest of the model domain. There is the potential for more removal occurring beyond the region modeled. The CDR from reduction of outgassing between October and May accounts for as much as 90% of total CDR simulated. Of the total, only 375 T CO_2 yr^{-1} (8%) was from the open shelf portion of the model domain. With shallow depths limiting vertical mixing, nearshore estuarine waters may provide a more rapid removal of CO_2 using alkalinity enhancement relative to deeper oceanic sites.

1. Introduction

At the current level of human emissions estimated at ≈40 GT (giga tons) CO_2 yr^{-1}, the target of limiting global warming to 1.5 °C–2.0 °C by 2100 set by the Paris Agreement of 2015 [1] will require proactive and deliberate CO_2 removal (CDR) of ≈10 GT CO_2 yr^{-1} from the atmosphere by mid-century, and ≈20 GT CO_2 yr^{-1} by mid-to-late century [2]. Oceanic capture of CO_2 from the atmosphere through air-sea gas exchange alone will not be sufficient [3, 4]. The natural processes would eventually reduce atmospheric CO_2 levels to nearly the preindustrial levels, but only at an unacceptably long timescale of ≈100–200 × 10^3 years [5–7]. Even after reducing emissions to net-zero levels, marine CDR efforts will be needed

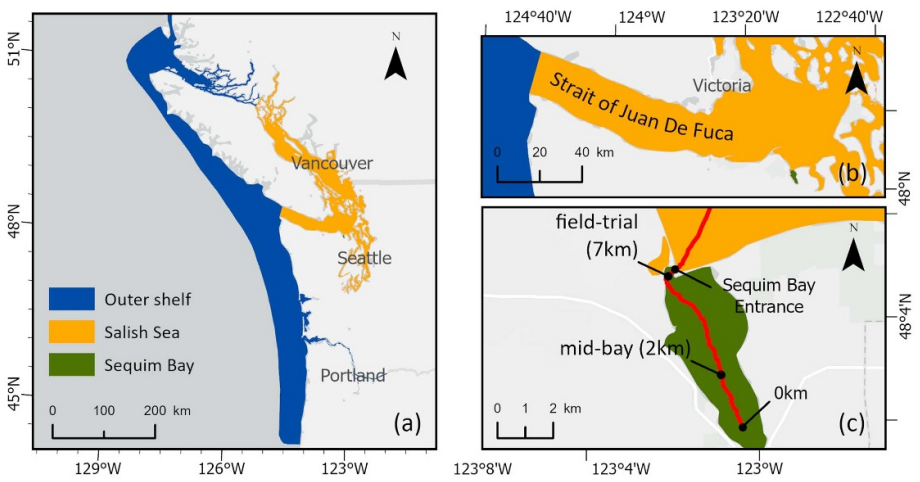

Figure 1. (a) Study area and Salish Sea Model domain divided by regions—Outer shelf (blue), Salish Sea (Yellow), and Sequim Bay (Green). (b) Location of Sequim Bay within Strait of Juan De Fuca region of the Salish Sea, (c) Sequim Bay with locations of field-trial and mid-bay sites. Red line is a transect through Sequim Bay.

to accelerate the oceanic carbon capture processes to shorter timescales of decades, to meet the 2100 target.

Ocean alkalinity enhancement (OAE) approach is an emerging technology, that has the potential to accelerate oceanic CO_2 uptake while providing the added benefit of local ocean acidity reduction. OAE techniques include direct addition of alkalinity through minerals such as pulverized carbonate/silicate rocks [8, 9], or releasing high-alkalinity aqueous streams (e.g. NaOH) generated via electrochemical splitting [10, 11] or electrodialysis [12–14]. Modeling studies ranging from simplified box models to spatially resolved models have examined the potential effectiveness of these alkalinity enhancement techniques [15–18]. Results in general indicate that extreme large-scale additions of alkalinity would be required to have a noticeable global scale effect on CDR. Keller *et al* [19] highlighted the challenge using scenarios limiting the alkalinity addition to ≈6 GT Ca^{2+} yr^{-1} as $Ca(OH)_2$, an amount that could be delivered by modern fleet of ships, resulting in only modest uptake of CO_2 (20 GT by 2030 and 180 GT by 2100). Ilyina *et al* [20] pointed out that alkalinization could still provide CO_2 uptake benefits on a nearshore subregional scale, and simultaneously help counteract local ocean acidification.

Simulated global-scale perturbations often do not accurately reflect the scale of the alkalinity enhancement strategies that will likely be employed in practice. Wang *et al* [21] tested a hypothetical total alkalinity (TA) release of 1.67×10^{10} mol TA yr^{-1} (equivalent to 667 950 T NaOH yr^{-1}) in Unimak Pass, Alaska using a 100 km grid size global-scale model, resulting in 639 905 T CO_2 yr^{-1} removed from the air. The authors noted that even for these seemingly large rates of TA release, the region over which surface pCO_2 mitigation was >10 ppm was limited to a single model cell. The scale of mixing zones associated with plumes from typical point source discharges ≈0.01–0.1 km^2 is considerably smaller than a typical regional/global ocean model cell ≈30–100 km^2. The coarse resolution of the large-scale models likely induces excessive numerical dilution due to instantaneous numerical mixing within the receiving cell. High resolution modeling, at the scale of near-field zone of mixing and tidal transport is needed to accurately resolve the expected benefits of practical full-scale deployment and to support feasibility assessment; design; siting; establishment of monitoring, reporting, and verification procedures; and evaluation of any potential ecosystem effects. Given costs of transportation, access to required electrical power, and potential ecosystem benefits, nearshore settings are an important consideration for the transition of technology from theory to practical deployment.

In this study, we examine the biogeochemical response of Sequim Bay, within the fjord-like estuarine waters of the Salish Sea, Washington, US (see figure 1) to OAE at the local scale of a planned field trial and hypothetical full-scale deployments. An existing electrodialysis system located onshore would deliver an enhanced-alkalinity stream at a TA of 2929 μmol kg^{-1} or 2997 milimol m^{-3} (mmol m^{-3}) and pH of 9 with ΔpH ≈ 1.06, and ΔTA ≈ 869 mmol m^{-3} relative to average ambient conditions) for the duration of one year. We use a regional scale model with sub-regional/site specific refinement to quantify the increase in CO_2 flux and pH over the domain. OAE via delivery of excess base in the form of hydroxide ions is expected to induce a rapid reduction in dissolved CO_2* [expressed collectively with H_2CO_3 as $CO_{2(aq)}$]. The resulting increase in the gradient between $CO_{2(air)}$ and $CO_{2(aq)}$ should provide a corresponding increase in

the net air-to-water CO_2 flux. However, equilibration occurs over a timescale of weeks or longer, during which turbulent mixing and dilution with ambient water with higher background $CO_{2(aq)}$ could rapidly diminish the gradient and rate of CO_2 capture away from the source. We use these simulations to assess how mixing and dilution impact CDR associated with OAE in a realistic nearshore estuarine setting relative to ideal open ocean conditions.

2. Methods and experimental design

2.1. Electrodialysis system—OAE field trial

A planned field trial of a bipolar electrodialysis (BPED) system at the US Department of Energy's Pacific Northwest National Laboratory, in Sequim Bay, Washington provided the setting and the opportunity for this modeling-based assessment. Figure 2 shows a schematic process diagram of the system developed by Ebb Carbon, Inc. consisting of withdrawal of seawater and electrochemical extraction of acid using BPED [12–14, 22, 23]. The extracted acid is diverted away for other beneficial uses and seawater with increased alkalinity is returned to surface waters.

The system is designed to generate a highly concentrated stream (mostly NaOH) at a pH $\approx$ 13.9. Blending with seawater is needed to reduce the pH to 9 prior to discharge in compliance with the local water quality standards, resulting in TA of 2929 μmol kg^{-1} (2997 mmol m^{-3}). Delivered at the field trial flow rate of 0.001 75 m^3 s^{-1}, this corresponds to TA addition of 0.164 Mmol yr^{-1}. Using CO2SYS [24], an ambient T = 14 °C, S = 30 psu, equilibrium pCO_2 of 398 ppm, and the ratio $\Delta CO_2/\Delta TA = 0.84$ [7, 23], the carbon capture potential for this added alkalinity is 6.1 ton yr^{-1}.

Alkalinity is a primary control for the carbon content in the ocean on long timescales, and the carbon capture potential is proportional to the alkalinity enhancement in seawater under equilibrium pCO_2 at the sea surface [7]. The addition of alkalinity to seawater results in a rapid reduction of $CO_{2(aq)}$ levels, governed by oceanic carbonate chemistry [22]. The net reactions are as follows,

$$OH^- + CO_{2(aq)} \rightarrow HCO_3^- \quad (1a)$$

$$OH^- + HCO_3^- \rightarrow H_2O + CO_3^{2-} \quad (1b)$$

Equations (1a) and (1b) occur over a short/immediate time scale [25].

Depleted $CO_{2(aq)}$ and bicarbonate (HCO_3^-) are replenished from the atmosphere over a longer time frame of weeks to months through air-sea CO_2 gas exchange described by equations (2a) and (2b) below,

$$CO_{2(air)} \rightarrow CO_{2(aq)} \quad (2a)$$

$$CO_{2(aq)} + H_2O + CO_3^{2-} \rightarrow 2HCO_3^-. \quad (2b)$$

Return to full equilibrium state with $CO_{2(aq)}$ replenished from air-to-sea transfer provides the theoretical maximum CO_2 capture. This assumes ideal conditions where added alkalinity remains at the surface and contributes fully towards CO_2 capture.

We leveraged the existing finite volume coastal ocean model (FVCOM [26]) hydrodynamics coupled to the FVCOM-ICM [27] biogeochemistry-based implementation of the *Salish Sea Model* [28, 29]. The model was refined within Sequim Bay region (see figure 1) to seamlessly resolve the mixing-zone-scale processes at the OAE site (25–100 m) where the process impacts will be most acute, to the local-scale (Sequim Bay wide) chronic impacts on ocean biogeochemistry that are relevant for assessing co-benefits such as local ocean acidification mitigation, to the larger regional-scale (Salish Sea wide) impacts on ocean carbon uptake and storage.

The model tracks the variations of TA and dissolved inorganic carbon (DIC) in the water column by considering the kinetic processes that contribute to the changes of TA and DIC acting as sources or sinks. Without a parameterization for carbonate mineral cycling, the modeled biological change in TA in the water column is proportional to the summation of the changes in NH_4^+ and NO_3^- concentrations due to primary production, remineralization of dissolved organic nitrogen constituents, denitrification, and sediment fluxes of NH_4^+ and NO_3^-. The model computes the DIC change by accounting for the changes in primary production, remineralization of dissolved organic carbon constituents, nitrification, denitrification, sediment fluxes, and air-sea exchange [30]. The model computes the CO_2 exchange between the atmosphere and the sea surface based on the equilibrium condition,

$$Q_c = K_v \left(CO_{2(aq)sat} - CO_{2(aq)surf}\right) A_{tce} \quad (3)$$

$$K_v = 0.251 W_{wind}^2 \left(\frac{660}{Sc}\right)^{1/2} \frac{24}{100}. \quad (4)$$

In equation (3), Q_c (mmol CO_2 d^{-1}) is the CO_2 gas exchange rate over A_{tce}. The area associated with the model grid node for tracer transport in FVCOM-ICM; $CO_{2(aq)surf}$ (mmol m^{-3}) is the concentration of $CO_{2(aq)}$ at the sea surface; $CO_{2(aq)sat}$ (mmol m^{-3}) is the saturated concentration of $CO_{2(aq)}$ at the sea surface; K_v (m d^{-1}) is the gas transfer velocity calculated based on the Wanninkhof (equation (4)) where W_{wind} (m s^{-1}) is the wind speed; Sc is the Schmidt number for CO_2 [31]. $CO_{2(aq)}$ is computed using CO2SYS [24] formulations built into FVCOM-ICM. Further, FVCOM-ICM computes pH as a state variable based on the TA, DIC, and rate constants from CO2SYS using Newton–Raphson iterative method, which is an adaptation of the approach used in pyCO2SYS [32]. The selection of K1, K2 and KSO_4 dissociation constants are based on the formulation of Lueker *et al* [33].

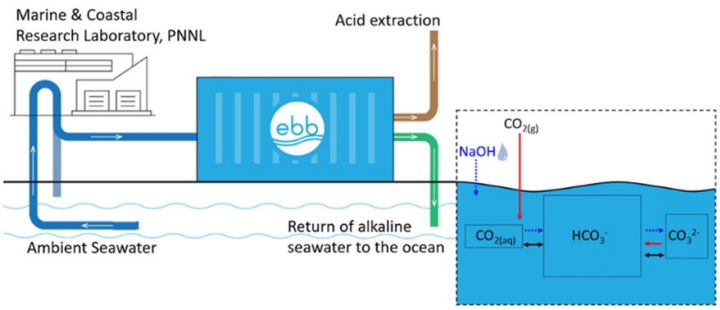

Figure 2. Schematic process flow diagram of the bipolar electrodialysis system installed in Sequim Bay, WA, USA (source: Ringham *et al* [23]).

In typical summer conditions when the ocean surface is undersaturated [$CO_{2(aq)surf} < CO_{2atm}$], the ocean absorbs CO_2 from the atmosphere resulting in a positive Q_c. For the Sequim Bay field trial with TA of 2929 μmol kg^{-1} the maximum carbon capture rate in the form of increase in CO_2 absorption flux (Q_c/A) is estimated at 2822 mmol CO_2 m^{-2} yr^{-1} at the source. This value was computed using the equilibrium condition-based gas exchange (equations (3) and (4) together with CO2SYS, and average summertime Salish Sea surface conditions ($T = 17$ °C, $S = 27$ psu, TA = 1914 μmol kg^{-1}, and DIC = 1758 μmol kg^{-1}) [34], corresponding pCO_2 level of 375 ppm, and average summer wind condition of 3.2 m s^{-1} for year 2014 from the University of Washington Weather Research Forecasting Model. However, in the winter, Salish Sea is supersaturated with $CO_{2(aq)}$ substantially exceeding the saturation levels [35]. The maximum CDR rate for the same alkalinity enhancement under the high-pCO_2 winter conditions ($T = 7$ °C, $S = 29$ psu, TA = 2020 μmol kg^{-1}, and DIC = 1971 μmol kg^{-1}), pCO_2 level of 685 ppm and average winter wind condition of 5.3 m s^{-1} for year 2014 is significantly (five-fold) higher with a reduction in outgassing CO_2 flux of 14 832 mmol CO_2 m^{-2} yr^{-1} at the release point. CO_2 flux determined with equations (3) and (4) is sensitive to lower T, higher TA, DIC, and particularly, wind and pCO_2.

2.2. Baseline, field trial and scale-up sensitivity tests

We designed four OAE scenarios, each with a two-year long simulation period consisting of continuous high alkalinity discharge for the first year followed by a second year with no discharge. The Sequim Bay discharge location and the greater Salish Sea have *e*-folding flushing times of about ten days, and about one year respectively [36]. A dynamic steady state within Sequim Bay is reached after ten days of discharge and a high alkalinity plume is continuously transported out into the Strait of Juan de Fuca and the Salish Sea. The effects of released excess residual alkalinity in the Salish Sea are accounted for until they are flushed out of the domain. The baseline conditions selected were based on Year 2014 model [37], with a validation completed previously, with zero discharge to serve as the reference for comparison to scenarios. The following scenarios were tested with enhanced TA addition in million mols (Mmol) over a 1 year duration (see figure 1 for site locations):

- SCN1 = field-trial site, 0.164 Mmol of TA added
- SCN2 = field-trial site, 164 Mmol of TA added
- SCN3 = mid-bay site, 0.164 Mmol of TA added
- SCN4 = mid-bay site, 164 Mmol of TA added

Scenarios SCN1 and SCN2 correspond to field trial site discharges, located near the western shoreline at the entrance of Sequim Bay. SCN3 and SCN4 evaluate the response to releasing enhanced-alkalinity seawater from the mid-bay site in quiescent conditions. SCN2 and SCN4 represent 1000 fold scale up from the field trial flow rate corresponding to potential full-scale deployment, with a realistic discharge rate of 40 million gallons per day (MGD) (1.75 m^3 s^{-1}), comparable to large municipal or industrial wastewater discharges in the region.

Only direct TA addition was considered, introduced as a TA flux (mmol s^{-1}) during these simulations. Addition of TA flux was only done in the first year, but the simulation continued over the second year with TA source shut off to allow residual enhanced TA within the domain to continue the CDR. The transports of mass and heat that could accompany industrial outfalls were not also parameterized to ensure that the physical circulation and characteristics within the baseline simulation remain directly comparable to those in the various scenarios.

3. Results and discussion

3.1. Nearfield mixing and dilution

Irrespective of the alkalinity delivery method, bulk release from a vessel or metered out through an outfall, the process of initial dilution from hydraulic mixing with the ambient is unavoidable. The concentrations during this near-field dilution phase reduce from the end-of-pipe levels by the dilution factor

that is directly proportional to ambient currents, inversely proportional to the flow rate, and affected by outfall/diffuser configuration. Dilution factor (ψ) is defined by the equation $\Delta Cf = \Delta C/\psi$ where ΔCf is the increase in ambient concentration after mixing in the field and ΔC is the difference between end of pipe concentration and the ambient.

In this case, relative to annual average ambient $TA_a = 2128$ mmol m^{-3}, the end-of-pipe TA (TA_e) corresponding to the scenarios of 2997 mmol m^{-3} corresponds to $\Delta TA = 869$ mmol m^{-3}. The final TA_f after mixing would be controlled by ψ. For a preliminary estimate, we used UM3, an analytical plume model that simulates jet and buoyancy induced dilution and mixing of fluids released through submerged outfalls [38]. Average ambient conditions ($T = 9.3$ °C, and $S = 30$) were used to estimate the expected nearfield dilution factors, within 100 m radius mixing zone (typical regulatory mixing zone size in Washington) for the respective scenarios. The nearfield dilutions for SCN1 and SCN2 at the shallow high current environment field-trial site were 388 and 13 respectively, while for SCN3 and SCN4 at the deeper mid-bay site, the dilutions are estimated at 336, and 65 respectively.

This is also reflected in the surface TA, pH, aragonite saturation state (Ω_{arag}), pCO_2, and ΔCO_2 flux plots shown in figure 3. At the low discharge rate of 0.164 Mmol, the dilutions are so high that the elevation of TA, pH, and Ω_{arag} levels, and reduction in pCO_2 are not detectable above ambient. However, at the full-scale deployment 164 Mmol, the spikes or drops in concentrations near the source location are the dominant feature. The increase in alkalinity (and pH) from the discharge causes a drop in pCO_2 resulting in an increase in CDR flux. The control exerted by the dilution process on TA, pH, and pCO_2 levels and therefore ΔCO_2 flux or CDR rate is seen in figure 3 (also see figurers S1 and S2 in supplementary materials).

Although $\Delta pH \approx 0.6$ is high near the source and has the potential to cause localized ecosystem impacts [39, 40], the pH levels of 8.6 is still well below the water quality protective standard of 9 in Washington, US, and drops rapidly to 8.1 or lower within the nearfield mixing zone ≈100 m (0.01 km^2), which lies within natural variability of pH in Sequim Bay [41]. The transects show that within Sequim Bay, there is elevation in background levels of pH and TA due to the longer residence and constrained flushing, but levels drop off further once the plume travels outside of Sequim Bay. While the CDR rate in Sequim Bay drops from the very high values near the source within the mixing zone, it is still elevated relative to baseline. CDR therefore continues at a lower rate, but over a much larger Sequim Bay area (13 km^2).

3.2. Change in CO_2 flux and pH in Sequim Bay

We focused our attention on the full-scale scenarios SCN2 and SCN4, the 1.75 m^3 s^{-1} discharges at a TA of 2997 mmol m^{-3}. These cases correspond to an addition of 165 Mmols yr^{-1} of TA. As shown in figure 3, in addition to the peak TA increase near the source, the sustained discharges achieve a dynamic steady state resulting in an elevation of the background TA levels over a larger zone of influence. Over this zone, the $CO_{2(aq)}$ levels in surface waters are reduced relative to baseline and the CO_2 capture process occurs at an enhanced level.

As discussed previously, most coastal estuaries including the Salish Sea are in a state of outgassing during the winter months [34, 35, 42]. The OAE effect on the gas exchange represents CDR irrespective of whether it helps enhance carbon capture from the atmosphere during the summer or reduce degassing to atmosphere from water during the winter. Figure 4 presents annual average ΔCO_2 flux in mmol CO_2 m^{-2} yr^{-1}. The mid-bay discharge allows greater retention of the enhanced alkalinity, resulting in greater increase in air-sea CO_2 flux within Sequim Bay (depth range: 0–38 m). The CDR benefit is realized over a long duration of (weeks to months) and covers a domain well beyond Sequim Bay, including the Salish Sea and the continental shelf to which alkalinity is exported. The annual average increases in CO_2 flux over the Sequim Bay domain are 1785 mmol CO_2 m^{-2} yr^{-1} (SCN2) and 3266 mmol m^{-2} yr^{-1} (SCN4). These differences are primarily due to location of SCN2 near the mouth of Sequim Bay in high current environment that allows faster transport of enhanced TA into the Salish Sea.

The addition of large volumes of basic water at the water quality standard limit of 9 pH to the Salish Sea also provides an immediate reduction of acidity broadly across the bay. Figures 3 and 5 show that the elevation of pH levels of up to 0.6 units appears feasible within the mixing zone near the mid-bay source for SCN4 after accounting for nearfield dilution. The annual average ocean acidification reduction for Sequim Bay is also significant with ≈0.1 units increase in pH. This improvement is comparable to the estimated reduction in pH of 0.11–0.06 due to global anthropogenic acidification processes in the region [43–45]. Qualitatively, these results indicate that application of OAE technology in protected environments with limited flushing has the potential to provide embayment-wide ocean acidification mitigation benefits. We note, however, that this increase in pH is accompanied by a drop in pCO_2 of over 200 ppm, which has the potential to affect the ecosystem through carbon limitation impacts to primary production [46].

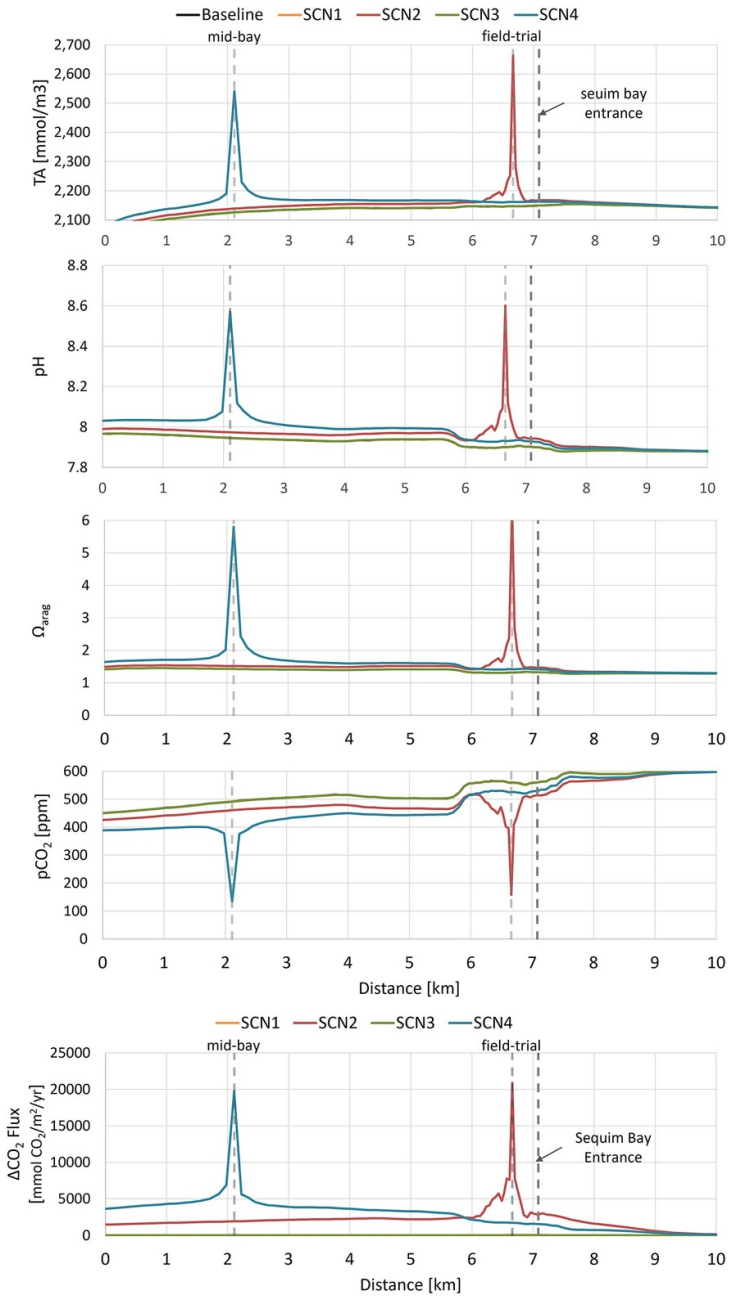

Figure 3. Total alkalinity (TA), pH, pCO_2, Ω_{arag}, and ΔCO_2 flux in the surface layer along the transect from southern end of Sequim Bay (0 m) through Sequim Bay entrance into the Strait of Juan De Fuca (see figure 1). Results are plotted for Baseline conditions along with the four scenarios averaged over a year of simulation. The mouth of Sequim Bay is marked by the dashed line.

3.3. CO_2 mass removal/capture in the Salish Sea

The CDR away from the source occurs at a slower rate but over a larger area and longer timeframe. Figure 6 shows a domain-wide distribution of enhanced alkalinity and higher ΔCO_2 flux for the full-scale mid-bay release scenario SCN4. While the domain-wide rates are a fraction of their levels relative to source location, the associated active area is considerably larger. The exported alkalinity from Sequim Bay mixes with the exchange flow in the Strait of Juan de Fuca and is transported landwards through the deeper layers, while alkalinity in the surface layers makes its way out to the continental shelf and to the Pacific Ocean through the open boundary. Figure 6 shows that CDR magnitudes over the shelf region with deeper waters drop significantly compared to the estuarine and relatively shallow stratified regions of the domain. The study area domain was divided into three regions (1) Outer shelf, (2) Salish Sea, and (3) Sequim Bay (see figure 1). Figure 7 shows composite bar charts representing total mass of CO_2 removed from the respective regions. The effects of residual alkalinity from the second year as it is flushed out of the system are also shown. The annual average alkalinity enhancement over the continental shelf and along the ocean boundary is reduced to trace levels <0.01 mmol m^{-3}.

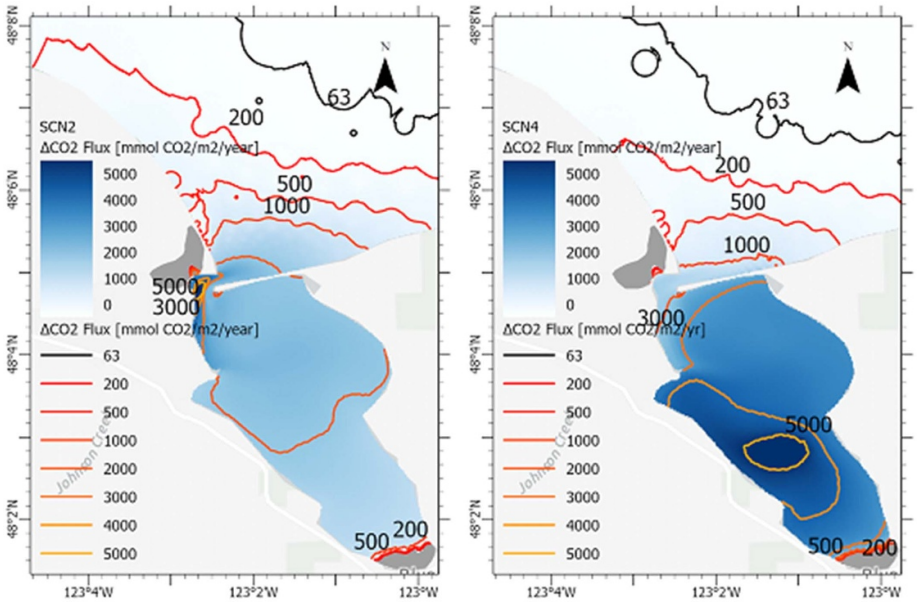

Figure 4. Change in air-to-water annual average CO_2 flux from OAE scenarios SCN2 (field-trial site) and SCN4 (mid-bay site). Enhanced CO_2 flux zone of influence is visible centered around the source locations for the full-scale TA release tests.

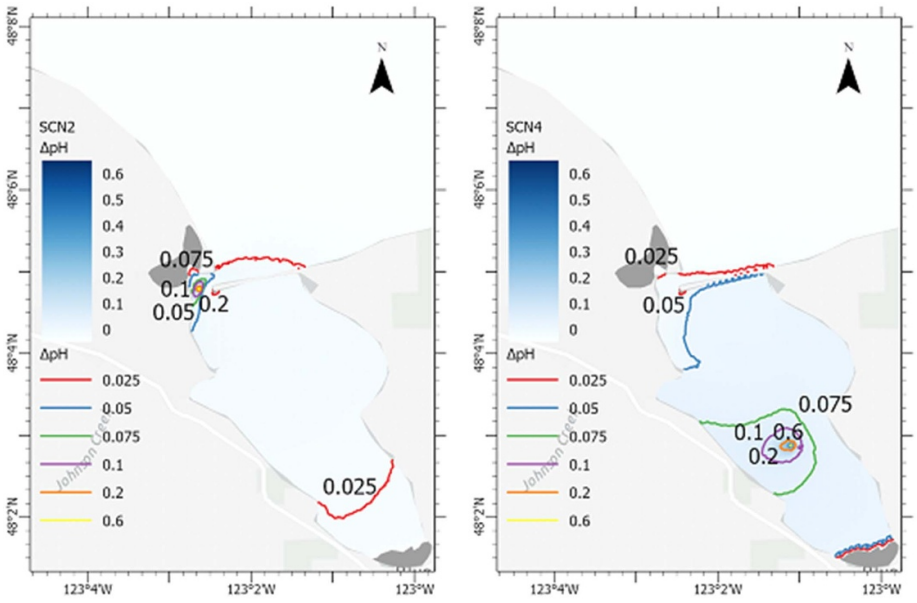

Figure 5. Average improvement in pH levels within Sequim Bay relative to the baseline showing increase in pH or reduction in acidity resulting from OAE scenarios SCN2 (field-trial site) and SCN4 (mid-bay site).

This alkalinity at a low-enhancement concentration is transported out of the domain through the open ocean boundary and will continue to capture carbon at a much lower rate asymptotically until reaching background TA concentrations.

The results show that although Sequim Bay occupies a small fraction of the study area (0.02%), it accounts for 24% and 45% of CDR relative to the entire domain for SCN2 and SCN4 respectively. The Salish Sea captures 66% and 47% of the CDR while the outer shelf accounts for 10% and 8% relative to the entire domain for SCN2 and SCN4 respectively. In addition, CDR associated with residual alkalinity is lower in the 2nd year at ≈38% relative to Year 1. This is consistent with the estimates of one-year *e*-folding Salish Sea flushing characteristics expected to flush down to 1/*e* (37%) level of alkalinity change in Year 2.

At a global scale, OAE is attributed a medium-high potential for CDR, with expectations of >0.1–1.0 GT CO_2 yr^{-1} [4]. At the upper limit of the range, at 1.0 GT CO_2 yr^{-1}, OAE represents a significant fraction of the 10 GT yr^{-1} global target for limiting global warming to 1.5 °C by 2100. This corresponds to a

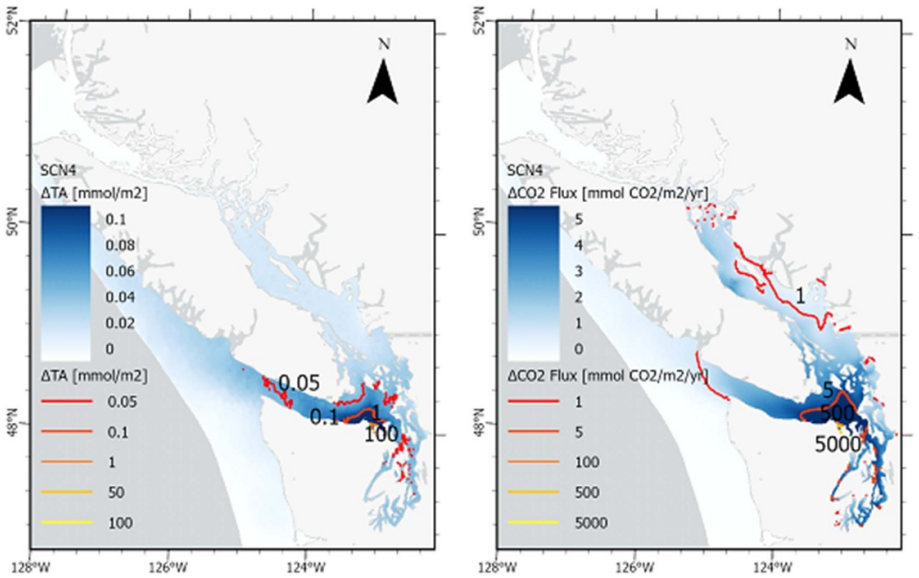

Figure 6. Enhanced alkalinity and CO_2 removal flux over the entire study domain from continuous high alkalinity discharge (SCN4) in Sequim Bay. The plot shows the effect of OAE extending beyond the confines of Sequim Bay release site to Salish Sea and the outer shelf.

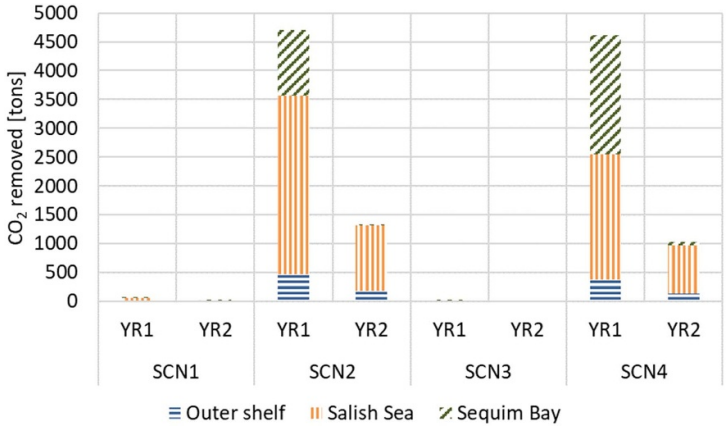

Figure 7. Mass of CO_2 removed through OAE scenarios SCN 1–4 distributed by regions within the study domain. Outer shelf—blue, Salish Sea (minus Sequim Bay)—yellow, and Sequim Bay—green. Stacked plots of CO_2 mass removed are shown for year 1 with the alkaline discharge and year 2 with discharge terminated.

global average increase in air-to-water CO_2 flux of ≈63 mmol m^{-2} yr^{-1} (using total ocean area [47] of 361.84 million km^2). Therefore, carbon capture must ideally occur at rates ⩾63 mmol m^{-2} yr^{-1} to have the potential to meet the demand for accelerated CDR and can serve as the OAE system design target and a point of reference for defining the optimum zone of influence.

The concern over the dilution control is straightforward in that physical mixing process may reduce the alkalinity concentration and/or divert the alkalinity away from the surface thereby reducing the carbon capture rates well below the ideal target. To illustrate this further, we used carbonate chemistry equilibrium kinetics (equations (1) and (2)) in CO2SYS, to compute the increase in CO_2 flux for varying dilution without considering vertical mixing. Baseline CO_2 flux was computed for $T = 14$ °C, $S = 30$ psu and, average alkalinity of 2096 μmol kg^{-1} and DIC of 2030 μmol kg^{-1} using equations (3) and (4). Nine different levels of enhanced alkalinities were simulated, ranging from 2400 to 4000 μmol kg^{-1}. The parameter values A_{tce} (1.0 m^2) and W_{wind} (5.0 m s^{-1}) were kept constant.

Figure 8 shows the sensitivity of the change in air-to-water CO_2 flux to dilution of TA. ΔQ_{ce} represents end-of-pipe peak change (increase) in CO_2 exchange rate relative to baseline (mmol CO_2 m^{-2} yr^{-1}). ΔQ_c is the increase in CO_2 flux after dilution. The plot shows that normalized CO_2 flux change declines with increasing dilution, indicating that the CDR rate reduces as the high alkaline plume travels away from the source and gets diluted due to ocean currents and tides-induced mixing.

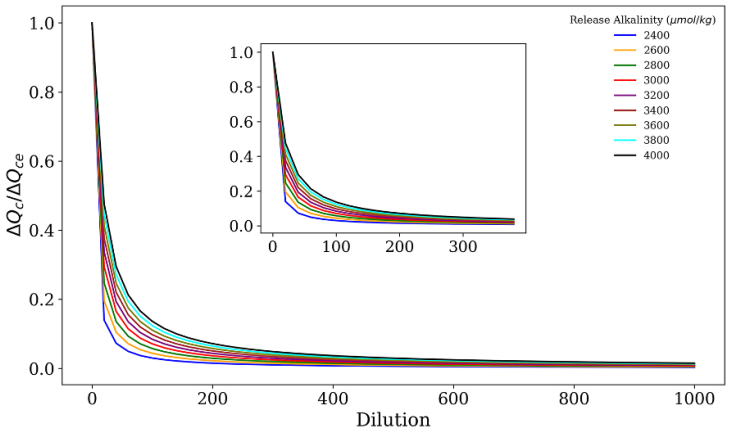

Figure 8. Normalized CO_2 flux change vs dilution for a tidally driven system in dynamic steady state.

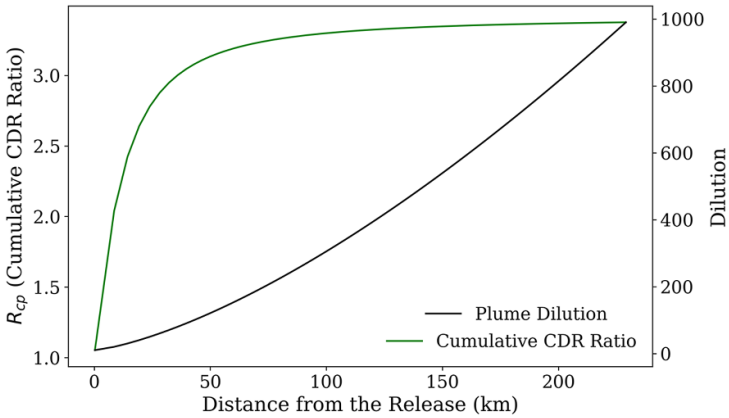

Figure 9. Cumulative CDR ratio (R_{cp}) showing the CO_2 removed by the enhanced TA plume relative to nearfield value, as it expands and transports to farfield with increasing dilution.

However, dilution due to lateral spreading has little influence on total CDR. While the lateral spreading increases dilution, the CDR occurs over a correspondingly larger area. This is shown in figure 9 using ratio R_{cp} defined as the cumulative CDR (farfield) at a distance x-km after dilution (ψ), relative to CDR (nearfield) at the source. Cumulative CDR in this example was computed using a hypothetical release of TA = 4000 μmol kg^{-1}, and assuming lateral spreading only using the 4/3rd power law (Brooks, 1960). In figure 8, relative increase in CO_2 flux $\Delta Q_c/\Delta Q_e$ drops rapidly by ≈90% within a short distance and a dilution ψ of >200. However, figure 9 shows that the cumulative CDR increases well up to over three fold increase, until $\psi = 900$ before plateauing out, in this case at distance of >50 km.

For the full-scale tests SCN2 and SCN4, the CO_2 flux drops below 63 mmol m^{-2} yr^{-1} within short a distance of ≈5 km (SCN2) and 8 km (SCN4) from the source locations, outside of Sequim Bay. Therefore, Sequim Bay and the 8 km boundary, shallow nearshore regions depths ≈0–40 m represents an optimum zone of influence for the scenarios tested that provides rapid CDR at above the global ideal. Interestingly, the CDR continues to be effective at lower rate but distributed over the larger Salish Sea area. It is not until the alkalinity plume is outside the shallower estuarine reaches, and out in the open ocean, that the CDR removal drops significantly, likely due to drop in surface TA concentrations from increased vertical diffusion in addition to lateral spreading relative to the confines of the Salish Sea. Relative to open ocean deeper waters, the estuarine stratified conditions and shallow depths limit the vertical mixing and dilution. This could be a benefit for coastal implementations, but further simulations would be required to directly address this possibility. It is worth noting that estuarine environments only represent a small fraction of the overall ocean surface area, and would therefore need large perturbations to be able to make quantitatively meaningful contributions to global CDR.

In addition, we found that OAE CDR benefit is more rapidly attained during the winter outgassing conditions typical of most estuaries and the Salish Sea. Here, the CDR benefit is realized in the form of reduction of outgassing through alkalinity addition. Table 1 below shows CO_2 removed from the Salish Sea

Table 1. Total CO_2 (tons) removed from the Salish Sea region using OAE scenarios SCN2 (field trial site) and SCN4 (mid-bay site), with enhanced TA additions of 164 million mols (Mmols) in 1 year.

Total CO_2 removed from the Salish Sea (T of CO_2 yr^{-1})[a]		
Summer (in-gassing period, April–September)	**SCN2**	**SCN4**
	363	404
2014 Summer—Salish Sea average: $T = 14$ °C, TA = 1884 mmol m^{-3}, DIC = 1695 mmol m^{-3}, pH = 8.2, pCO_2 = 263 ppm		
Winter (out-gassing period, October—March)	**SCN2**	**SCN4**
	3926	3872
2014 Winter—Salish Sea average: $T = 9$ °C, TA = 1977 mmol m^{-3}, DIC = 1888 mmol m^{-3}, pH = 7.9, pCO_2 = 523 ppm		
Total	4289	4276

[a] Total CO_2 from one year model simulation for SCN2 and SCN4.

region of the model domain in tons for the full-scale tests separated into summer in-gassing vs. winter out-gassing periods. Nearly 90% of the CDR for all scenarios is associated with a reduction of outgassing during the months from October to March in the Salish Sea. The difference is due to sensitivity of the of air-water CO_2 exchange rate to lower winter temperatures and higher TA, DIC, and pCO_2, and stronger wind.

4. Conclusion

The results show that an enhanced-alkalinity stream released to surface waters at the local water quality standards limit of 9 pH, TA 2997 mmol m^{-3} s^{-1} at full-scale deployment (at flow rates typical of large municipal or industrial wastewater outfalls ≈40 MGD) can provide significant marine CDR of ≈0.4 KT CO_2 yr^{-1} from the atmosphere. However, when carbon capture benefits of reduced degassing are included, the value increases to ≈4.2 KT CO_2 yr^{-1}.

The results highlight the control exerted on the quantity of CDR by the mixing and dilution of the added alkalinity plume, demonstrating a sharp decline in CDR rates per unit area with increasing dilution. Carbon removal at higher dilution is not affected if it simply occurs over larger area at a proportionally lower rate. This is the case in shallow estuarine waters where mixing is restricted to lateral spreading limited by depth. However, as the plume spreads to deeper oceanic water, the diffusion over depth could potentially result in a decrease in the CDR rate.

In naturally outgassing estuarine conditions stronger CDR benefit may be through reduction of degassing of CO_2 to the atmosphere. The CDR associated with reduction of outgassing between October and March accounts for as much as 90% of total simulated CDR in Salish Sea.

In addition, our analysis indicates that the application of OAE in protected environments with limited flushing has the potential to provide embayment-wide local acidification mitigation benefits. The results showing improvement in pH levels comparable to the estimated reduction in pH of 0.11–0.06 due to global anthropogenic acidification processes in the region is a very encouraging finding.

These results indicate that nearshore estuarine waters may provide a better performance and attractive setting for full-scale OAE systems relative to deeper oceanic sites. While the results are promising, the biogeochemical feedback and impacts on biota of releasing enhanced-alkalinity streams at large flow rates in estuarine environments are largely unknown and require further investigation. As shown in panel 3 of figure 3, the drop in pCO_2 by more than 200 ppm (locally) could lead to severe carbon limitation and has the potential impact primary production.

It is important to note that the model does not consider loss of DIC from 'runaway precipitation'. As shown in panel 4 of figure 3, average Ω_{arag} levels peak at ≈6 and limited to a small footprint of ≈100 m. However, daily maximum values can reach as high as 15 and can have a larger footprint ≈500 m in diameter (see supplementary material figures S3 and S4). The assumption is that associated outfall diffuser will be designed to provide sufficient initial dilution such that aragonite saturation state (Ω_{arag}) remains below the threshold of 5 and the concern managed within the constraints of an authorized mixing zone [48]. Intermittent dosing could be another option to address this risk. Thresholds of concern for runaway precipitation are a subject of ongoing research [23].

The simulated TA variations only consider the effects of NH_4^+ and NO_3^- changes due to biogeochemical processes. The Salish Sea however does exhibit blooms of biocalcifiers such as coccolithophores [49] that also affect TA. While the model used is locally refined, the Sequim Bay resolving version is based on previously calibrated models [28, 36], it has not yet been validated using data from Sequim Bay. Due to these limitations, there is a high

level of uncertainty, particularly during outgassing in the estuarine setting.

Data availability statement

The data and model results that support the findings of this study will be made available upon request through the *Salish Sea Modeling Center* data portal at URL/DOI: https://ssmc-uw.org/salish-sea-modeling-center/data-portal/

Acknowledgments

This research was primarily supported by the Climate Works Foundation Grant Number 22-2361. Partial support was received from the US Department of Energy's Waterpower Technologies Office Laboratory Research Program at Pacific Northwest National Laboratory (PNNL). BRC and MMS thank the National Oceanographic Partnership Program (NOPP) under the National Oceanic and Atmospheric Administration's Ocean Acidification Program (Crossref Funder ID: 100018228; ROR ID: https://ror.org/02bfn4816) award to University of Washington CICOES. The CICOES and PMEL contributions are Numbers 2024-1381 and 5645, respectively.

Conflict of interest

MDE is Co-Founder and Chief Scientific Advisor at Ebb Carbon, Inc., MCR, TP, and KT are employees of Ebb Carbon.

ORCID iDs

Tarang Khangaonkar https://orcid.org/0000-0003-2881-9467
Su Kyong Yun https://orcid.org/0009-0004-9505-7778
Nicholas D Ward https://orcid.org/0000-0001-6174-5581
Lenaïg G Hemery https://orcid.org/0000-0001-5337-4514
Krti Tallam https://orcid.org/0000-0002-4509-4157

References

[1] United Nations Framework Convention on Climate Change 2015 Adoption of the Paris agreement *Report No.* FCCC/CP/2015/L.9/Rev.1 (available at: http://unfccc.int/resource/docs/2015/cop21/eng/l09r01.pdf)
[2] NASEM (National Academies of Sciences, Engineering, and Medicine) 2019 *Negative Emissions Technologies and Reliable Sequestration: A Research Agenda* (The National Academies Press)
[3] Global Carbon Project 2021 Global Carbon BudgET 2021 (available at: www.globalcarbonproject.org/carbonbudget/index.htm)
[4] NASEM (National Academies of Sciences, Engineering, and Medicine) 2022 *A Research Strategy for Ocean-based Carbon Dioxide Removal and Sequestration* (The National Academies Press) (https://doi.org/10.17226/26278)
[5] Falkowski P *et al* 2000 The global carbon cycle: a test of our knowledge of earth as a system *Science* **290** 291–6
[6] Friedlingstein P *et al* 2023 Global carbon budget *Earth Syst. Sci. Data* **15** 5301–69 Humphreys M P, Lewis E R, Sharp J D and Denis P 2022 *Geosci. Model. Dev.***15** 15–43
[7] Renforth P and Henderson G 2017 Assessing ocean alkalinity for carbon sequestration *Rev. Geophys.* **55** 636–74
[8] Kheshgi H S 1995 Sequestering atmospheric carbon dioxide by increasing ocean alkalinity *Energy* **20** 915–22
[9] Gore S, Renforth P and Perkins R 2019 The potential environmental response to increasing ocean alkalinity for negative emissions *Mitig. Adapt. Strateg. Glob. Chang.* **24** 1191–211
[10] Rau G H 2008 Electrochemical splitting of calcium carbonate to increase solution alkalinity: implications for mitigation of carbon dioxide and ocean acidity *Environ. Sci. Technol.* **42** 8935–40
[11] Willauer H D, DiMascio F, Hardy D R and Williams F W 2014 Feasibility of CO_2 extraction from seawater and simultaneous hydrogen gas generation using a novel and robust electrolytic cation exchange module based on continuous electrodeionization technology *Ind. Eng. Chem. Res.* **53** 12192–200
[12] Eisaman M D, Parajuly K, Tuganov A, Eldershaw C, Chang N and Littau K A 2012 CO_2 extraction from seawater using bipolar membrane electrodialysis *Energy Environ. Sci.* **5** 7346
[13] de Lannoy C-F, Eisaman M D, Jose A, Karnitz S D, DeVaul R W, Hannun K and Rivest J L B 2018 Indirect ocean capture of atmospheric CO_2: part I. Prototype of a negative emissions technology *Int. J. Greenhouse Gas Control* **70** 243–53
[14] Eisaman M D, Rivest J L B, Karnitz S D, De Lannoy C-F, Jose A, DeVaul R W and Hannun K 2018 Indirect ocean capture of atmospheric CO_2: part II. Understanding the cost of negative emissions *Int. J. Greenhouse Gas Control* **70** 254–61
[15] Chuck A, Tyrrell T, Totterdell I J and Holligan P M 2005 The oceanic response to carbon emissions over the next century: investigation using three ocean carbon cycle models *Tellus* B **57** 70–86
[16] Ferrer-González M and Ilyina T 2016 Impacts of artificial ocean alkalinization on the carbon cycle and climate in Earth system simulations *Geophys. Res. Lett.* **43** 6493–502
[17] Burt D J, Fröb F and Ilyina T 2021 The sensitivity of the marine carbonate system to regional ocean alkalinity enhancement *Front. Clim.* **3** 624075
[18] Schwinger J, Bourgeois J T and Rickel W 2024 On the emission-path dependency of the efficiency of ocean alkalinity enhancement *Environ. Res. Lett.* **19** 074067
[19] Keller D P, Feng E Y and Oschlies A 2014 Potential climate engineering effectiveness and side effects during a high carbon dioxide emission scenario *Nat. Commun.* **5** 3304
[20] Ilyina T, Wolf-Gladrow D, Munhoven G and Heinze C 2013 Assessing the potential of calcium-based artificial ocean alkalinization to mitigate rising atmospheric CO_2 and ocean acidification *Geophys. Res. Lett.* **40** 5909–14
[21] Wang H, Pilcher D J, Kearney K A, Cross J N, Shugart O M, Eisaman M D and Carter B R 2023 Simulated impact of ocean alkalinity enhancement on atmospheric CO_2 removal in the Bering Sea *Earth's Future* **11** e2022EF002816
[22] Eisaman M D *et al* 2023 Assessing the technical aspects of ocean-alkalinity enhancement approaches A Oschlies, A Stevenson, L T Bach, K Fennel, R E M Rickaby, T Satterfield, R Webb and J-P Gattuso ed *Guide to Best Practices in Ocean Alkalinity Enhancement Research* vol 2-oae2023 (Copernicus Publications, State Planet) p 3
[23] Ringham M, Hirtle N, Shaw C, Lu X, Herndon J, Carter B and Eisaman M 2024 A comprehensive assessment of electrochemical ocean alkalinity enhancement in seawater: kinetics, efficiency, and precipitation thresholds

(EGUsphere) (available at: http://doi.org/10.5194/egusphere-2024-108)
[24] Lewis E and Wallace D W R 1998 *Program Developed for CO_2 System Calculations, ORNL/CDIAC-105, Carbon Dioxide Information Analysis Center* (Oak Ridge National Laboratory, U.S. Department of Energy) (https://doi.org/10.15485/1464255)
[25] Zeebe R E and Wolf-Gladrow D 2001 *CO_2 in Seawater: Equilibrium, Kinetics, Isotopes* vol 65 (Gulf Professional Publishing)
[26] Chen C, Liu H and Beardsley R C 2003 An unstructured, finite-volume, three-dimensional, primitive equation ocean model: application to coastal ocean and estuaries *J. Atmos. Ocean. Technol.* **20** 159–86
[27] Kim T and Khangaonkar T 2012 An offline unstructured biogeochemical model (UBM) for complex estuarine and coastal environments *Environ. Modelling Softw.* **31** 47–63
[28] Khangaonkar T, Nugraha A, Xu W, Long W, Bianucci L, Ahmed A, Mohamedali T and Pelletier G 2018 Analysis of hypoxia and sensitivity to nutrient pollution in Salish Sea *J. Geophys. Res.* **123** 4735–61
[29] Khangaonkar T and Yun S K 2023 Estuarine nutrient pollution impact reduction assessment through euphotic zone avoidance/bypass considerations *Front. Mar. Sci.* **10** 1192111
[30] Bianucci L, Long W, Khangaonkar T, Pelletier G, Ahmed A, Mohamedali T, Roberts M, Figueroa-Kaminsky C, Deming J W and Miller L A 2018 Sensitivity of the regional ocean acidification and the carbonate system in Puget Sound to ocean and freshwater inputs *Elem. Sci. Anth.* **6** 22
[31] Wanninkhof R 2014 Relationship between wind speed and gas exchange over the ocean revisited *Limnol. Oceanogr.* **12** 351–62
[32] Humphreys M P, Lewis E R, Sharp J D and Pierrot D 2022 PyCO2SYS v1.8: marine carbonate system calculations in Python *Geosci. Model Dev.* **15** 15–43
[33] Lueker T J, Dickson A G and Keeling C D 2000 Ocean pCO_2 calculated from dissolved inorganic carbon, alkalinity, and equations for K1 and K2: validation based on laboratory measurements of CO_2 in gas and seawater at equilibrium *Mar. Chem.* **70** 105–19
[34] Alin S R, Newton J A, Feely R A, Greeley D, Curry B, Herndon J and Warner M 2024 A decade-long cruise time series (2008–2018) of physical and biogeochemical conditions in the southern Salish Sea, North America *Earth Syst. Sci. Data* **16** 837–65
[35] Murray J W, Roberts E, Howard E, O'Donnell M, Bantam C, Carrington E, Foy M, Paul B and Fay A 2015 An inland sea high nitrate-low chlorophyll (HNLC) region with naturally high pCO_2 *Limnol. Oceanogr.* **60** 957–66
[36] Premathilake L and Khangaonkar T 2022 Explicit quantification of residence and flushing times in the Salish Sea using a sub-basin scale shoreline resolving model *Estuar. Coast. Shelf Sci.* **276** 108022
[37] Khangaonkar T, Nugraha A, Yun S, Premathilake L, Keister J E and Bos J 2021 Propagation of the 2014–2016 northeast pacific marine heatwave through the Salish Sea *Front. Mar. Sci.* **8** 787604
[38] Frick W E, Roberts P J W, Davis L R, Keyes J, Baumgartner D J and George K P 2003 Dilution models for effluent discharges 4th edition (visual plumes) (Ecosystems Research Division, NERL, ORD U.S. Environmental Protection Agency) (available at: www.epa.gov/hydrowq/dilution-models-effluent-discharges-visual-plumes-4th-edition)
[39] Oberlander J L, Burke M E, London C A and MacIntyre H L 2024 Assessing the impacts of simulated ocean alkalinity enhancement on viability and growth of near-shore species of phytoplankton (EGUsphere) (available at: http://doi.org/10.5194/egusphere-2024-971)
[40] Goldenberg S U *et al* 2024 Viability of coastal fish larvae under ocean alkalinity enhancement: from organisms to communities (EGU sphere) (available at: http://doi.org/10.5194/egusphere-2024-286)
[41] Jones K, Hemery L, Ward N, Regier P, Ringham M and Eisaman M 2024 Biological response of eelgrass epifauna, Taylor's sea hare (Phyllaplysia taylori) and eelgrass isopod (Idotea resecata), to elevated ocean alkalinity *Preprint* (https://doi.org/10.5194/egusphere-2024-972)
[42] Li M, Guo Y, Cai W-J, Testa J M, Shen C, Li R and Su J 2023 Projected increase in carbon dioxide drawdown and acidification in large estuaries under climate change *Commun. Earth Environ.* **4** 68
[43] Feely R A, Alin S R, Newton J, Sabine C L, Warner M, Devol A, Krembs C and Maloy C 2010 The combined effects of ocean acidification, mixing, and respiration on pH and carbonate saturation in an urbanized estuary *Estuar. Coast. Shelf Sci.* **88** 442–9
[44] Feely R A, Carter B R, Alin S R, Greeley D and Bednaršek N 2024 The combined effects of ocean acidification and respiration on habitat suitability for marine calcifiers along the west coast of North America *J. Geophys. Res.* **129** e2023JC019892
[45] Pelletier G, Bianucci L, Long W, Khangaonkar T, Mohamedali T, Ahmed A and Figueroa-Kaminsky C 2017b Salish Sea model ocean acidification module and the response to regional anthropogenic nutrient sources. Salish Sea model sediment diagenesis module *Publication No.* 17–03-009 (Washington State Department of Ecology) (available at: https://apps.ecology.wa.gov/publications/documents/1703009.pdf)
[46] Bednaršek N, Pelletier G, van de Mortel H, García-Reyes M, Feely R and Dickson A Unifying framework for assessing sensitivity for marine calcifiers to ocean alkalinity enhancement identifies winners, losers and biological thresholds—importance of caution with precautionary principle (EGUsphere) (available at: http://doi.org/10.5194/egusphere-2024-947)
[47] Charette M A and Smith W H F 2010 The volume of Earth's ocean *Oceanography* **23** 112–4
[48] Moras C A, Bach L T, Cyronak T, Joannes-Boyau R and Schulz K G 2022 Ocean alkalinity enhancement—avoiding runaway $CaCO_3$ precipitation during quick and hydrated lime dissolution *Biogeosciences* **19** 3537–57
[49] Esenkulova S, Suchy K D, Pawlowicz R, Costa M and Pearsall I A 2021 Harmful algae and oceanographic conditions in the Strait of Georgia, Canada based on citizen science monitoring *Front. Mar. Sci.* **8** 725092